## ON-LINE APPENDIX

### *Neurovascular Phantom Setup*

The schematic showing the phantom setup for the study is shown in On-line Fig 3.

### *Neurovascular Phantom Validation*

The human head attenuation varies greatly due to differences in various factors, including age, sex, weight, and location. For angiography system testing and evaluation, various commercial anthropomorphic head phantoms such as SK150 (The Phantom Laboratory, Greenwich, New York), RS-240T (Radiology Support Devices, Long Beach, California), and PBU-50 (Kyoto Kagaku, Torrance, California) are available. These phantoms simulate x-ray attenuation of the head along with its anatomic features. However, for intervention-procedure simulation, they lack the ability to simulate cerebral vasculature with various diseases and the pulsatile blood flow through such vasculature. With the neurovascular phantom presented in this work, different disease pathology and different interventional treatments can be simulated by changing the 3D-printed models.

The attenuation of the neurovascular phantom used in this study was compared with that in the above 3 commercially available anthropomorphic phantoms using the automatic exposure control of the x-ray machine. The automatic exposure control adjusts exposure parameters (eg, kilovolt, milliampere, and millisecond) so that "constant" exposure reaches the image receptor independent of "patient" attenuation. This feature ensures similar image quality with varying beam attenuation. With the automatic exposure control turned on, if the entrance skin exposures are similar for different patient models, it can be concluded that the x-ray attenuation of the models is similar.

To assess the primary beam attenuation, we imaged the neurovascular phantom using the FPD mode of the new detector system with a 2.5-inch FOV at the image receptor, at 3 different C-arm angles. The Source to Image receptor Distance (SID) was set at 100 cm. At each C-arm angle, exposures were performed under fluoroscopy, DA, and DSA modes. The exposure parameters of kilovolt, milliampere, and milliseconds for each acquisition were determined by the x-ray machine using its automatic exposure-control algorithm. For these parameters, the entrance air kerma at a reference point 60 cm from the source was calculated. At the same FOV, SID, and similar C-arm angles, the above acquisitions were repeated for each anthropomorphic phantom and the entrance air kerma was calculated. The On-line Table shows the calculated entrance air kerma for each phantom with fluoroscopic, DA, and DSA exposures. From the On-line Table, it can be seen that the entrance air kerma due to the automatic exposure-control–selected exposure parameters of the neurovascular phantom is similar to that in the 3 different anthropomorphic phantoms. This finding indicates that the attenuation of the neurovascular phantom is similar to the 3 anthropomorphic head phantoms.


**ON-LINE FIG 1.** Photograph of the new x-ray imaging system. The detector has both a regular-resolution 194-$\mu$m pixel FPD mode and a high-resolution 76-$\mu$m pixel HiDef mode in 1 single unit.

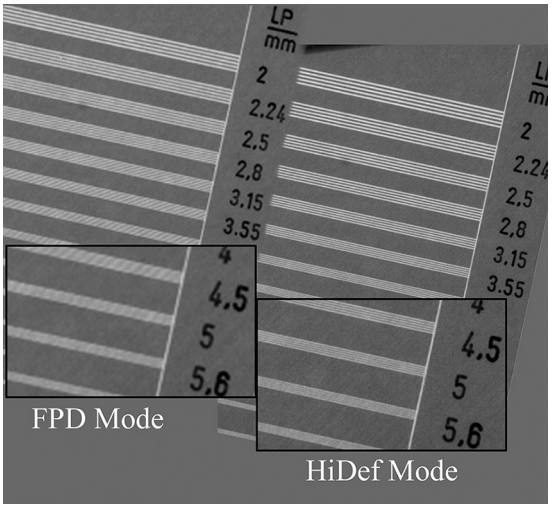


**ON-LINE FIG 2.** Image of a line pair phantom acquired using the 194-$\mu$m pixel FPD detector mode and the 76-$\mu$m pixel higher resolution HiDef mode. For the reader to visualize the difference between the 2 modes, the line pair images above 4.5 line pairs/mm are magnified. In the FPD image, due to its larger pixel size, only line pairs up to 2.5 line pairs/mm can be imaged without any loss in information. In the HiDef image, due to its smaller pixel size, line pairs up to 5.6 line pairs/mm can be imaged without any loss in information. Note that the reader is advised to zoom the display to enable a better appreciation of the comparisons.

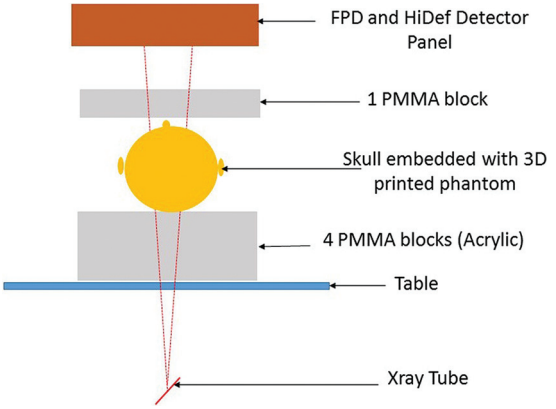


**ON-LINE FIG 3.** Anteroposterior projection (frontal C-arm view) of a neurovascular phantom for simulation of clinical views of PED deployment. The phantom simulates bone attenuation (skull), tissue attenuation (total of five 1-inch polymethylmethacrylate blocks; PMMA, Codman Cranioplastic, Raynham, Massachusetts), and diseased cerebrovasculature (3D-printed phantom embedded inside the skull). The detector panel was placed 10 cm from the top PMMA block. The lateral C-arm view of a biplane angiography system was simulated by rotating just the skull containing the 3D-printed phantom on its side.

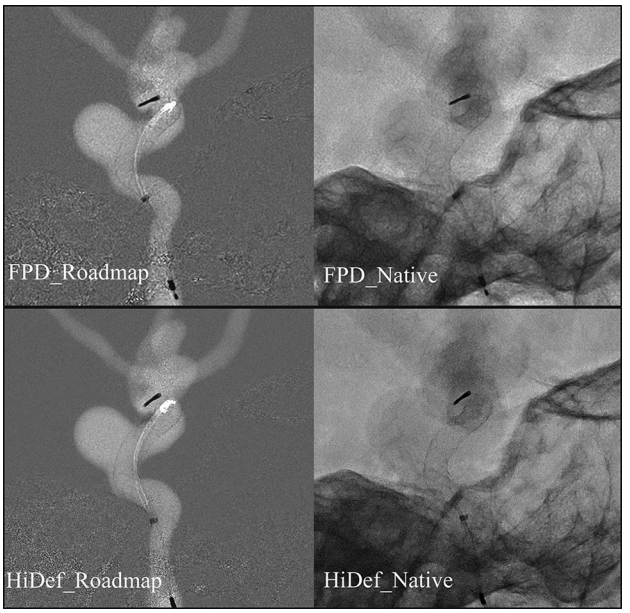


**ON-LINE FIG 4.** Sample of an image-sequence pair acquired under fluoroscopic conditions. During clinical neurointerventions, both roadmap and native images complement each other and are displayed and visualized simultaneously. To mimic this feature, we showed the raters both roadmap and native deployment image sequences simultaneously for each detector mode on 1 monitor, each at their native resolution (1024 × 1024 pixels), with similar brightness and contrast. The average reference point air kerma per frame for fluoroscopy was calculated to be 0.02 mGy for the FPD mode and 0.03 mGy for the HiDef mode. Note that the reader is advised to zoom the display to enable a better appreciation of the comparisons.

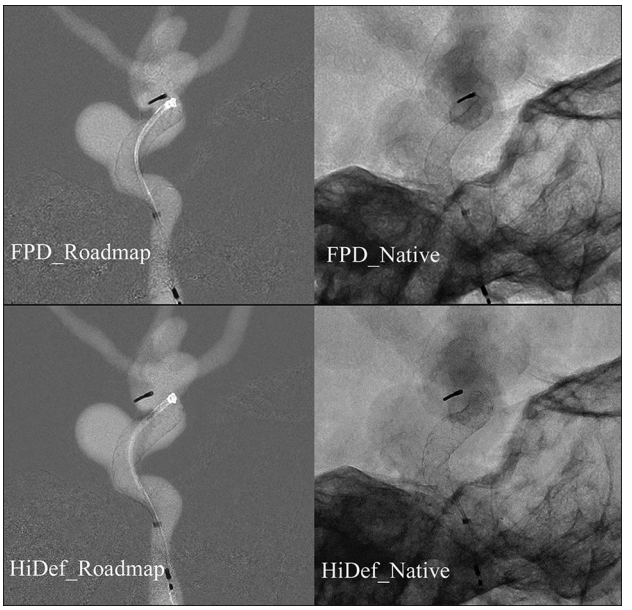


**ON-LINE FIG 5.** Sample of a single image-sequence pair acquired under DA exposures. During clinical neurointerventions, both roadmap and native images complement each other and are displayed and visualized simultaneously. To mimic this feature, we showed the raters both roadmap and native deployment image sequences simultaneously for each detector mode on 1 monitor, each at their native resolution (1024 × 1024 pixels), with similar brightness and contrast. The average RP air kerma per frame for DA was calculated to be 0.16 mGy for the FPD mode and 0.17 mGy for the HiDef mode. Due to more quanta reaching the detector, the image quality is improved for both the FPD and HiDef modes compared with On-line Fig 4. The amount of information available in the HiDef images is higher than that in the FPD images. Note that the reader is advised to zoom the display to enable a better appreciation of the comparisons.

**On-line Table: Entrance air kerma at 60 cm from the source calculated from the parameters selected by the AEC for commercial anthropomorphic phantoms and the custom neurovascular phantom at 3 C-arm angles each**

| Anthropomorphic Head Phantoms | Entrance Air Kerma (mGy) | | |
|---|---|---|---|
| | Fluoroscopy | DA | DSA |
| SK150 | 0.16 | 0.29 | 2.58 |
| | 0.15 | 0.28 | 2.52 |
| | 0.10 | 0.24 | 2.47 |
| RS-240T | 0.17 | 0.29 | 2.46 |
| | 0.17 | 0.29 | 2.53 |
| | 0.12 | 0.25 | 2.23 |
| PBU-50 | 0.16 | 0.29 | 2.24 |
| | 0.18 | 0.29 | 2.19 |
| | 0.07 | 0.22 | 2.26 |
| Average | 0.14 | 0.27 | 2.39 |
| Neurovascular phantom | 0.14 | 0.27 | 2.56 |
| | 0.16 | 0.29 | 2.35 |
| | 0.11 | 0.24 | 2.52 |

**Note:**—AEC indicates automatic exposure control.